Applying full-azimuth depth imaging in the local angle domain to delineate hard-to-recover hydrocarbon reserves

Alexander Inozemtsev[1], Zvi Koren[1]* and Alexander Galkin[2] present an alternative imaging system, which provides much richer information on the subsurface image points.

Introduction

Hard-to-recover hydrocarbon reservoirs lie at great depths, in complex geological conditions. They are characterized by complex structures, low fluid permeability and a low oil and gas recovery ratio. In Russia today, about 60% of the potential oil and gas fields are located in this type of reservoir. These include hydrocarbon deposits in the Paleozoic basement (pre-Jurassic basement) of Western Siberia, subsalt carbonate sediments under salt dome tectonics, and carbonate and terrigenous deposits in the Volga region and Eastern Siberia. The exploration of these reservoirs benefits from a new, full-azimuth angle domain approach to seismic processing and imaging. This new technology can provide a more detailed depth image of the entire structural-tectonic reservoir skeleton, and a more accurate forecast of the main rock properties of the reservoirs.

Conventional seismic depth imaging tools, such as ray-based or beam-based Kirchhoff migrations, applied to rich azimuth seismic data, normally generate multi-azimuth offset-domain common image gathers (CIGs). These are further used for anisotropic velocity model determination and for the characterization of reservoir properties, such as fracture systems. In these types of migrations, the input data is first binned into specific surface offset/azimuth geometrical groups, such as offset vector tiles (OVT), azimuthal sectors or planner spirals, depending on the acquisition pattern. Each set of binned data is then independently migrated, with the final CIGs being simply a collection of individual images. However, in many cases, particularly when studying hydrocarbon reservoirs below complex geological areas and along steep inclined layers, the offset/azimuth CIGs do not provide the required information (in terms of accuracy and resolution, for example) to achieve the above mentioned goals. Unlike subsurface imaged events along the angle domain CIGs, which indicate 'true' local reflectivities, the reflection image events along the offset domain CIGs can be only considered a rough approximation of the 'true' reflectivities. Obviously, the accuracy and reliability of the offset domain CIGs are strongly compromised when imaging below complex geological areas with complex wave phenomena. One of the main drawbacks of offset domain imaging, especially in complex geological areas, is its inability to deal with the actual multi-pathing waves which are naturally handled within angle domain imaging. Moreover, the surface azimuths of the offset domain CIGs represent the directions between sources and receivers along the acquisition surface, which can be considerably different from the actual in-situ azimuth along the inclined reflectors.

In this work we use an attractive alternative imaging system, the EarthStudy 360 Imager (Koren and Ravve, 2011), which provides much richer information on the subsurface image points compared to any other available seismic imaging/migration system. In this imaging system, the surface recorded seismic data are simultaneously mapped (downward propagated using an advanced ray-based solution) to the subsurface and binned into high-resolution, multi-dimensional tables at each subsurface grid point. Each bin is characterized by the spatial location coordinates of a given subsurface image point and by a given central ray pair (incident/scattered slowness vectors), arriving to the image point from a given source and scattered up to a given receiver, forming a local four-dimensional angle system, referred to as the local angle domain (LAD). Two of the four LAD angles indicate the apparent directivity (dip and azimuth) of the given ray pair, while the other two indicate the opening angle and azimuth between the ray pair. Hence, the output of the system consists of 5D LAD image gathers generated at the inline/crossline locations. The vertical axis of these image gathers indicates the fine-grid depth locations, and the other four axes indicate the above mentioned directivity and reflectivity LAD angles.

The imaged amplitudes of the directivity components within the LAD (directional) gathers provide the ability to decompose the imaged data into specular (most energetic) components (associated with the specular direction/s) and non-specular (different types of diffraction) components. Specular energy is mainly used to enhance subsurface image/structural continuity, while non-specular (diffraction) components are used to enhance discontinuous objects, such as small faults, edges and tips, and even fine fracture systems.

The imaged amplitudes of the reflectivity components (specular energy) within the LAD gathers (full- azimuth reflection angle gathers), provide rich information about the in-situ full-azimuth angle domain residual moveouts (translated to traveltime errors along the central ray pairs) to be used for updating/refining the background depth velocity model (e.g., anisotropic tomography).

[1] Paradigm | [2] JSC ZPG – RusOil
* Corresponding author, E-mail: Zvi.Koren@pdgm.com

Once the velocity model is updated and the seismic events along the image gathers are relatively flat (from all azimuths and angles), the amplitude preserved image events along the full-azimuth reflection gathers are used for azimuthally varying amplitude analysis vs. angles (AVAZ) and amplitude inversion to obtain impedances and rock properties.

Main stages

The LAD depth imaging technology was used in two oil fields with hard-to-recover reserves: Western Siberia and the Volga region. The process included:

1. Amplitude preserved time processing
2. Building an initial isotropic depth velocity model
3. Conversion from isotropic model to anisotropic VTI using anisotropic tomography
4. Anisotropic (VTI) depth Kirchhoff migration

LAD imaging

1. 3D ray tracing to study the illumination of the target depth objects, taking into account the anisotropy/heterogeneity of the velocity model and estimating the suitability of the data for full-azimuth studies. This includes estimation of the main illumination parameters for deep horizons, optimal fold, distribution of the opening angle and azimuthal characteristics, horizontal distance and azimuthal displacement (migration aperture parameters) and reliability of the parameters studied.
2. LAD migration and creation of full-azimuth directional angle gathers.
3. Extraction of information about dip, azimuth and continuity (DAC) of the reflecting subsurface elements (e.g., horizons and faults).
4. LAD migration and creation of full-azimuth reflection angle gathers.
5. Study of the change in velocity and reflection amplitudes as a function of the opening angle and azimuth direction (VVAZ and AVAZ analysis).
6. Selection of information from directional gathers to enhance the image quality of the specular (continuous horizons) and diffraction (discontinuous objects) components. In particular, performing a weighted sum of the specular component and adaptive removal of the specular energy from the directional gathers (Koren, 2016).
7. Interactive analysis of azimuthally varying residual moveouts (RMOz) characterized by three effective parameters: Azimuth of the low second-order NMO velocity ('slow' azimuth), the residual NMO velocity in the direction of the slow azimuth, and the residual NMO velocity in its perpendicular direction ('fast' azimuth). The difference between the two residuals is indicated by the effective anisotropic intensity.
8. Generalized Dix-type inversion, where any successive top and bottom horizon's global effective parameters are converted to local (layer) effective parameters. Finally, the local effective parameters are inverted to interval azimuthally anisotropic, horizontally transverse isotropy (HTI) parameters.
9. Constrained azimuthally varying amplitude vs. angle (AVAZ) analysis to obtain further high-resolution azimuthally varying intensity, reliability, and more precise information about the directivity of the existing fracture systems or dominant stress.

Analysis of the seismic and geological results of LAD imaging

Western Siberia

Figure 1 compares the results of a depth image obtained using Kirchhoff migration technology with an image that uses the LAD depth migration technology at a site in Western Siberia. From a geological point of view, potential reservoirs with hard-to-recover reserves in the pre-Jurassic rock complex (often called the pre-Jurassic Paleozoic basement) are considered for further drilling. The Paleozoic basement in the target area is represented by a complex set of terrigineous, volcanic and magmatic rocks and carbonates with different lithologies (schists, granites, volcano-sedimentary strata, siliceous-clastic strata, dolomites, and other carbonates) and has systems of disturbance: faults, mega-cracks, meso-fractures and micro-fractures. Reservoirs are characterized by a complex block structure of fractured or fractured-cavernous type, with predominantly low permeability.

In the results presented in Figure 1, it is important to note that for the same signal spectrum (or the same vertical resolution), fundamentally different seismic depth images are obtained both in terms of boundaries and disturbances, and in terms of geological interpretation. The seismic horizons resulting from LAD imaging are smoother and easier to track. The unconformity between the sedimentary deposits of the Mesozoic and Paleozoic

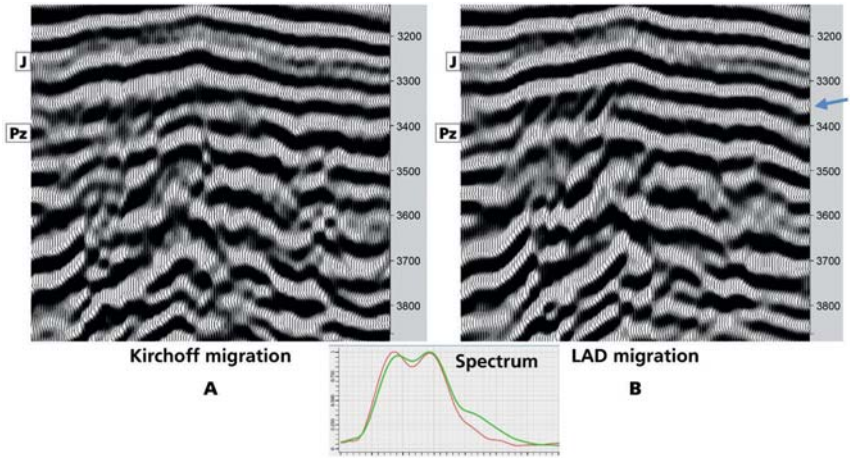

Figure 1 Delineation of fractured reservoirs with hard-to-recover reserves (HTRR) in the Pz basement. Comparison of depth images between (A) Kirchhoff migration and (B) LAD depth processing. The blue arrow indicates the unconformity boundary between the Mesozoic and Paleozoic sedimentary complex.

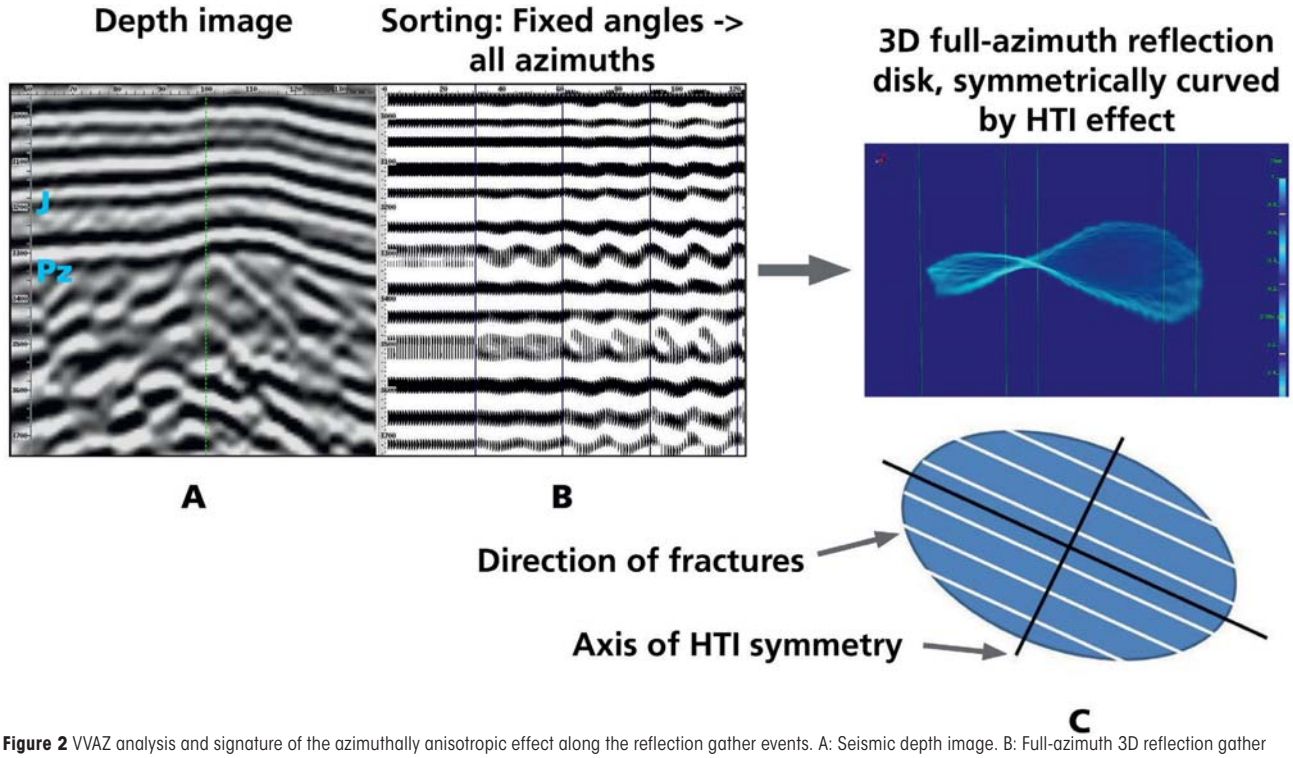

Figure 2 VVAZ analysis and signature of the azimuthally anisotropic effect along the reflection gather events. A: Seismic depth image. B: Full-azimuth 3D reflection gather with manifestation of the azimuthally anisotropic effects. C: 3D full-azimuth reflection disk symmetrically curved by the azimuthally anisotropic effect ('saddle' geometry).

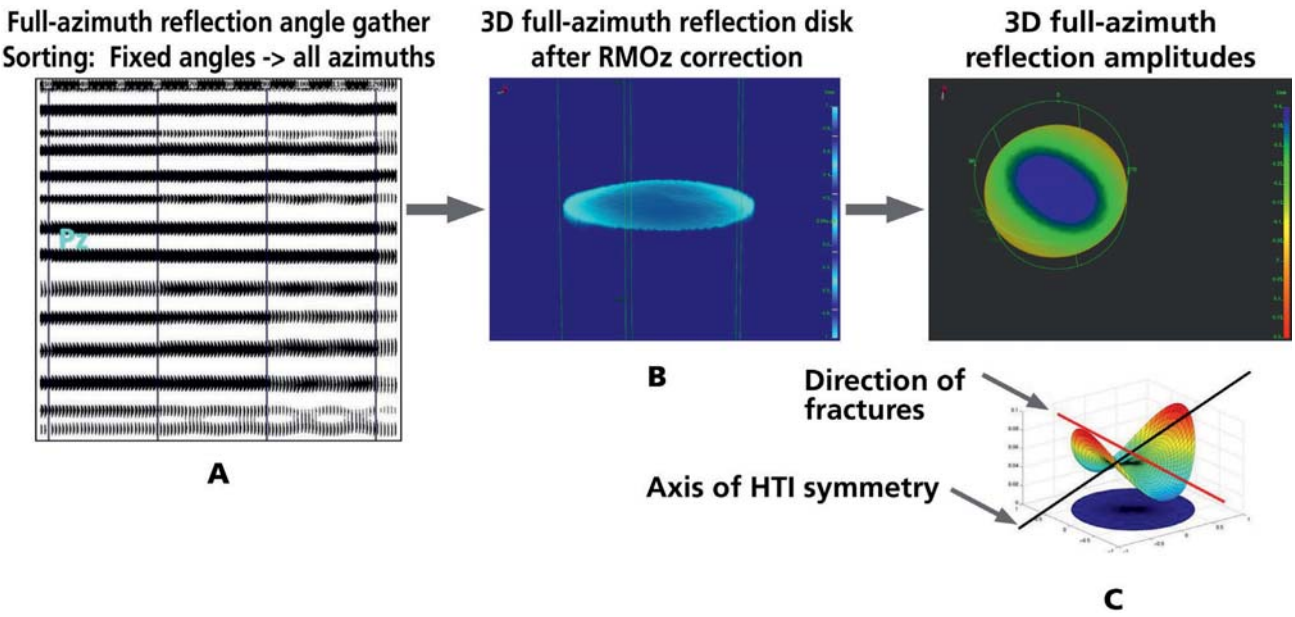

Figure 3 AVAZ analysis and signatures of azimuthally anisotropic effect in amplitudes on reflection angle gathers in LAD imaging. A: Full-azimuth 3D reflection angle gather after RMOz correction. B: 3D full-azimuth reflection disk after RMOz correction. C: Schematic drawing of the formation of an elliptic law of azimuthal amplitude variation.

sedimentary complex is also clearer. In the left part of image (B) at the top of the Paleozoic basement, below the unconformity boundary, a system of subvertical and inclined reflections is clearly distinguishable, manifesting itself as alternating inclined reflecting fragments ('tiles' – T. Olneva, 2010). In the lower part of the Paleozoic basement, the inclined seismic horizons and system of subvertical faults are also better distinguished.

Figure 2 shows the result of full-azimuth LAD imaging, which confirms the fractured nature of the Paleozoic basement deposits. Figure 2B shows the result of VVAZ analysis along the full-azimuth reflection gathers. The azimuthal variation (oscillation) of the reflected events is clearly seen at the bottom of the target formation, indicating azimuthal anisotropic velocity distribution: The NMO velocity is azimuthally dependent (elliptic shape). The lower peaks of the oscillated reflection event indicate the azimuth of the low NMO velocity, whereas the upper picks indicate the azimuth of the high NMO velocity. Next, the three global NMO effective parameters (azimuth of the slow, low and high NMO velocities) are transformed (generalized Dix-type approach) into local effective parameters using the top and

bottom effective parameters. These parameters indicate the actual azimuthal anisotropic effect at the given layer.

The oscillated reflection events are then flattened using the RMOz effective parameters (Figures 3A and B), enabling the performance of azimuthally varying amplitude vs angle (AVAz) analysis (Figure 3C).

According to the full-azimuthal equation for the variation in reflection coefficients as a function of azimuth (Ruger, 1998), in the presence of horizontally transverse isotropy (HTI), the shape of the azimuthally varying amplitude variation is also an ellipse.

Below is a schematic drawing of the formation of an elliptic form of amplitude variation in the case of HTI anisotropy. The shape of the amplitude variation in the full-azimuth version (as in the case of velocity changes) is also similar to the 'saddle' geometric surface. The maximum change in the amplitudes corresponds to the direction of the HTI symmetry axis. It is important to note that the results of both types of analysis, VVAZ (local parameters) and AVAZ, with correct full-azimuth depth imaging, should be consistent. The agreement (correlation) of both types of analysis increases the reliability of the prediction of the stressed state of the rocks, and zones of increased fracturing in potential hydrocarbon reservoirs.

Figures 4 and 5 show the results of imaging and focusing the diffraction/scattered components in directional gathers in order to isolate heterogeneities in the Paleozoic basement. At the same time, the geological problem of segregating seismic data from disturbance systems is solved primarily by the formation of a complete seismic image of the structural-tectonic skeleton.

When selecting the diffraction and corner waves, we used a modified processing graph based on adaptive removal of the specular energy. On the full-azimuth directional gather (Figure 4B), the diffraction/corner waves are narrow-azimuth. On a

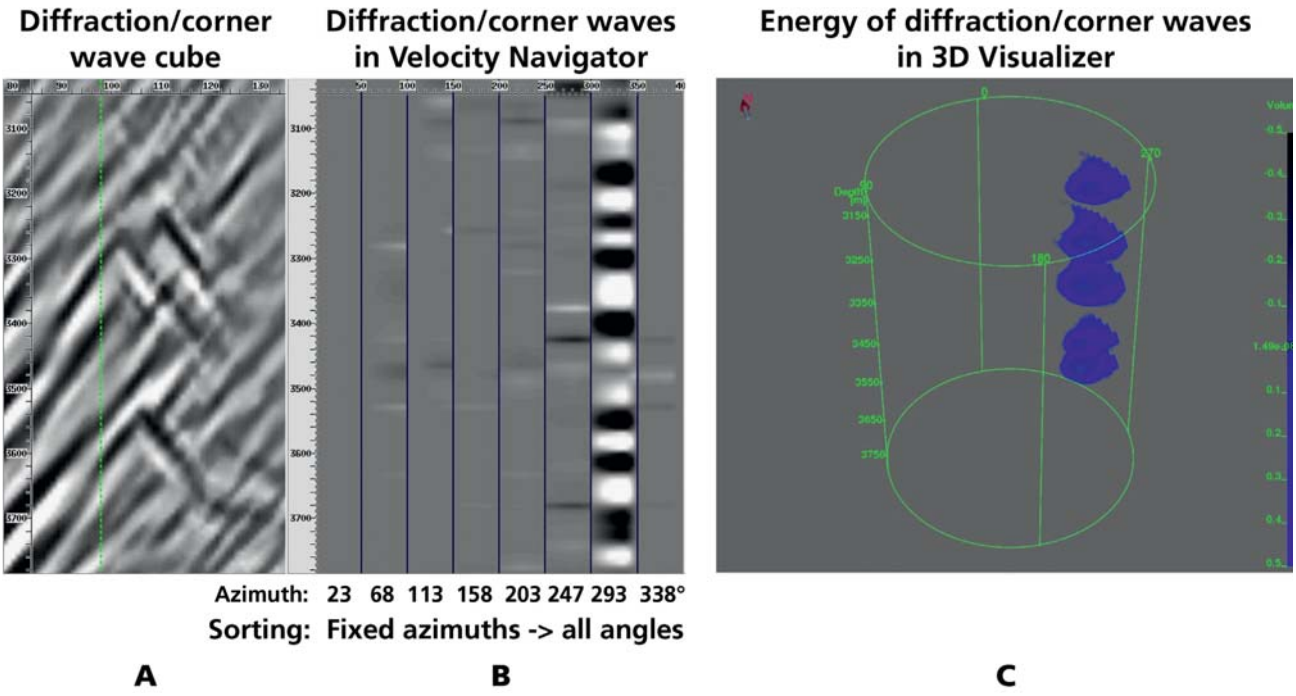

Figure 4 Registration of diffracted/corner waves in the Pz basement: Full interval of the Paleozoic basement (Carbon-Devon divisions). The energy (amplitudes) of diffraction waves from directional gather. A: Cube of diffraction/corner wave components. B: 3D full-azimuth directional gather after selection and removal of the specular component in the range of incidence angles from 20 - 40°.

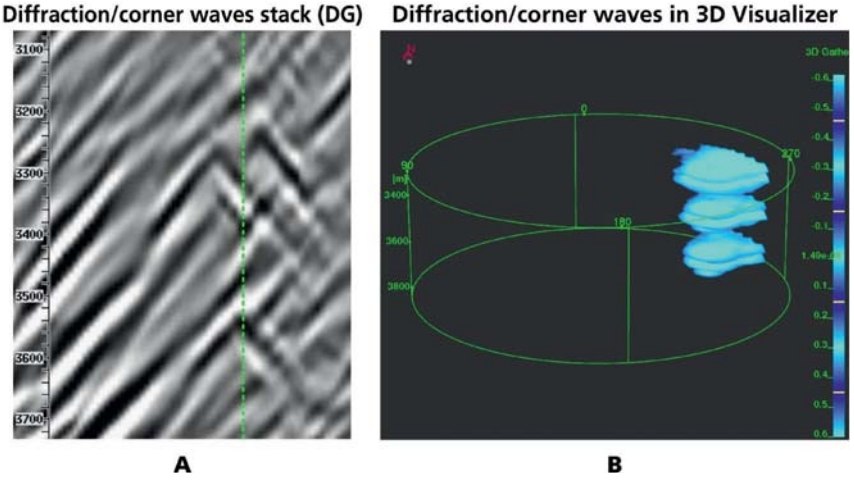

Figure 5 Signatures of diffracted/corner waves in the Pz basement: Lower interval of the Paleozoic basement (Carbon-Devon divisions). The energy (amplitudes) of diffraction waves from directional gather. A: Cube of diffraction/corner wave components. B: 3D full-azimuth directional gather after selection and adaptive removal of the specular component in the range of incidence angles from 20-40°.

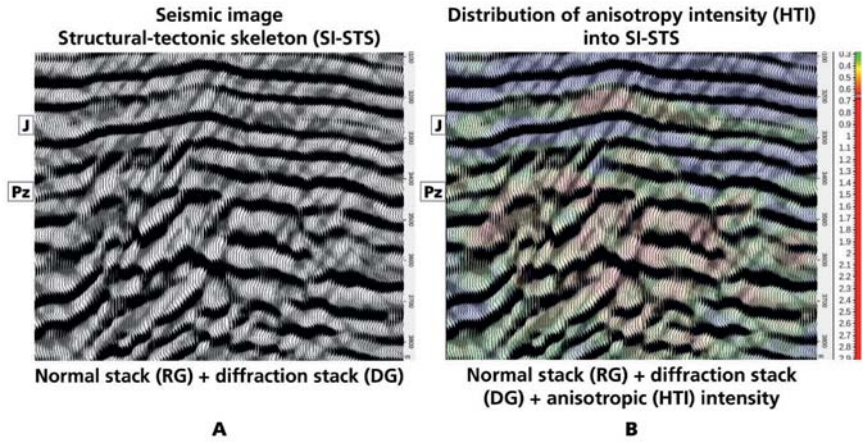

Figure 6 Delineation of fault systems and fractured reservoirs with hard-to-recover reserves in the Pz basement. A: Seismic image of structural-tectonic skeleton (SI-STS). B: Distribution of the azimuthally anisotropic intensity into SI-STS. 3D inline.

Figure 7 Fractures (X-Y) in nature. An array of carbonates (photo courtesy of Mikhail Yerchenkov, 2016.).

specific directional gather, they are distributed along the trend azimuth direction 293° from the north (clockwise) crosswise to the lateral strike of the fault system. Therefore, it is easy to predict that the fault system has a dominant azimuthal direction along the strike about 200° from a northerly direction. In addition, the fault systems are inclined with an incidence angle of about 45° from the vertical.

Figure 6 shows the section of the cube formed by imposing a LAD normal cube obtained from reflection gathers and a diffraction cube obtained from directional gathers. One can see a seismic image of two oblique counter systems of disturbances (faults and mega-cracks) of the X-type and an additional subvertical system of faults. Together, all of the disturbance systems form a seismic image of the tectonic geological skeleton. On the Earth's surface, there is a sufficient number of natural systems of faults and cracks (Figure 7). When a seismic image of the tectonic skeleton is superimposed over seismic horizons, a complete seismic image of the structural-tectonic skeleton (SI-STS) can be obtained. This image is a clear and reliable basis for the final interpretation and construction of the geological model.

The most interesting phenomena for the integrated interpretation and prediction of fractured reservoirs are the stress/fracture density cubes calculated by the AVAZ inversion, which are then combined with the seismic image of the structural-tectonic skeleton (SI-STS) (Figure 6B). In the combined image, the block structure of the Paleozoic basement and the clear differentiation of blocks with increased and decreased stress/fracture density values are clearly visible. This, in turn, is controlled by fault systems.

It is known that in the Jurassic period, vertical tectonic movements took place in the southeastern regions of Western Siberia. The Paleozoic paleo-protrusions with the greatest contrast grew throughout the entire Jurassic period. In the Jurassic, the destruction of elevated areas of the Paleo-relief exceeded their growth. An analysis of the seismic data brings us to the conclusion that the most contrasting paleo-protrusions of the pre-Jurassic basement developed during the Jurassic period, and their relative 'growth', were accompanied by the active formation of faults (V.A. Kontorovich, 1999). It is also known that post-Jurassic tectonic processes included the formation of different systems of disturbances owing to the activity of compressive and tensile forces, ultimately forming the paleo-structural form of the Paleozoic basement.

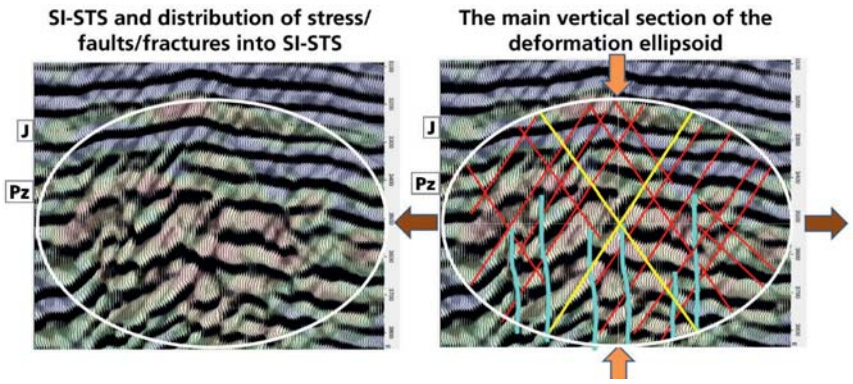

Figure 8 Geomechanical model of the formation of systems of disturbances at unilateral subvertical and horizontal volumetric stress state of rocks. Light brown arrows – maximum compressive forces. Dark brown arrows – maximum tensile force. Yellow lines – the circular sections of the deformation ellipsoid. Red lines – a system of crossing disturbances (faults and fractures). Blue lines – breakaway faults and fractures.

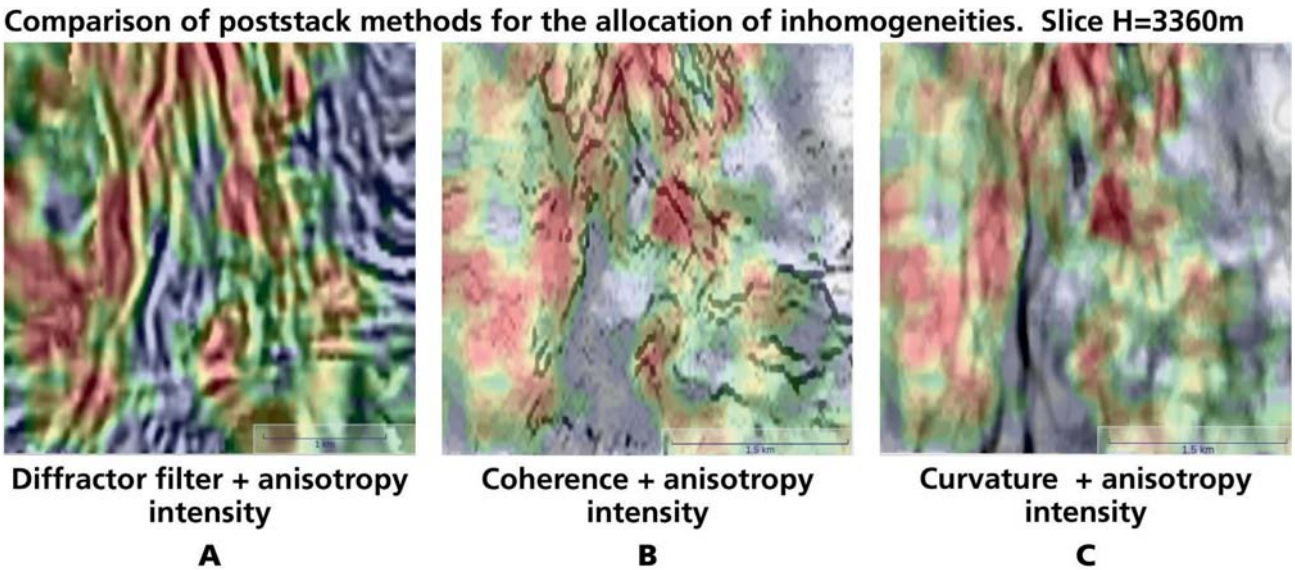

Figure 9 Comparison of prestack and poststack methods for the allocation of heterogeneities. Depth slice H=3360 m. A: Prestack technology of adaptive removal of the specular energy. B: Poststack technology for obtaining Coherence Cube for the LAD normal cube. C: Poststack technology for obtaining Curvature Cube for the LAD normal cube.

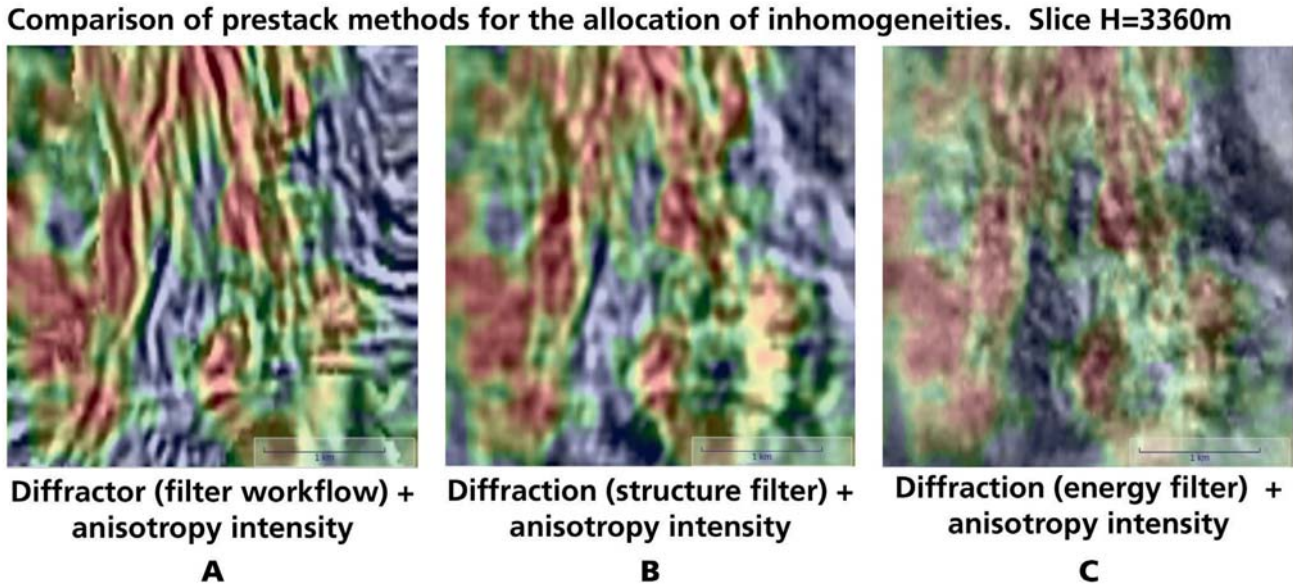

Figure 10 Comparison of prestack methods for allocating heterogeneities. Slice H=3360 m. A: New prestack technology for selection and adaptive removal of specular energy. B: Prestack technology using structural filters (Dip, Azimuth). C: Prestack technology which uses only weight energy filters to separate the diffraction components.

According to the laws of geomechanics, the destruction of rocks through disturbances, in the form of faults and fractures created by external forces, occurs simultaneously in several directions. These disturbances may be divided into two main groups: The first (cleavage faults and cracks) are formed along the circular sections of the deformation ellipsoid. Such disturbances are usually rectilinear, extended and tightly compressed, and have a slope of 30-50° relative to the (small) axes of symmetry of the deformation ellipsoid. They can be inclined equally across layers with different lithologies. The second group is composed of breakage faults and cracks, which are formed perpendicular to the main (large) axis of symmetry of the deformation ellipsoid. Such disturbances are short, unrestrained, and with no displacement tracks, having a curved shape and somewhat wide opening.

Based on the available literature, the compressive or tensile forces are oriented in the vertical section of the deformation ellipsoid. In this case, two systems of shearing faults/mega-fractures and one system of breaking faults are formed.

Figure 8 shows a variant of a similar geomechanical model combined with a real seismic integrated section (SI-STS and azimuthally anisotropic intensity). In this interpretation, the compressive forces in the vertical direction form two opposing systems of shearing faults (with an angle of inclination relative to the vertical of about 45°). In this interpretation, it is not difficult to predict the direction of the main normal stresses that form the disturbance systems shown in the seismic data. This information is also useful for understanding the geological structure and tectonic processes occurring in different geological eras.

Figure 9 compares the effectiveness of different technologies in allocating faults and mega-fractures, with overlapping information about the intensity of the azimuthal anisotropy (stress/fracture density). The depth slice corresponds to the upper part of the Paleozoic basement. When comparing the results of different poststack technologies, one can see that the Coherence Cube (B) identifies a system of faults, but the image is fuzzy and discontinuous. Faults on the Curvature Cube (C) are more continuous and rectilinear. The highest quality, most detailed fault images are obtained using the directional gathers with adaptive removal of the specular energy. This result also shows the best consistency between the fault system and the distribution of HTI isotropy intensity.

Figure 10 compares different prestack technologies for allocating disturbances with overlaid information about azimuthally anisotropic intensity (stress/fracture density). When comparing the results, one can see that the heterogeneity cube (C) obtained using weight energy filters to track disturbances (faults/mega-cracks) is inferior to the cube of heterogeneities obtained using structural filtering (B). The highest-quality result for allocating the system of faults/mega-cracks and consistency with azimuthally anisotropic intensity is result (A), which uses prestack adaptive removal of specular energy.

Figures 11 and 12 show the process of seismic imaging of the structural-tectonic skeleton (SI-STS), where at each stage another image characteristic is added. In Step 1, the specular component cube (A) and diffraction component cube (B) were obtained separately (using the directional filter applied to the directional gathers). An opacity tool was used to emphasize the contrast between the two components. In Step 2, the specular and diffraction image cubes were combined to produce a co-visualized seismic SI-STS image. In Step 3, the SI-STS cube was combined with a cube of azimuthally anisotropic intensity. This integrated volumetric image provided a good background for further in-depth interpretation towards constructing the final geological model of the study area.

Creation of a 3D seismic image of the structural-tectonic skeleton – Step 1

Note also that separate blocks (yellow circle) with anomalous anisotropy values, and with very small values that are clearly separated by the system of disturbances (faults/mega-fractures) and structural horizons, are clearly shown in the integrated cube (Figure 12).

Analysing the change in the structural-tectonic skeleton (SI-STS) and the azimuthally anisotropic intensity cube with depth in the volume led to the following conclusions. The system of disturbances (faults and mega-cracks) is inherited from the top down and is formed mainly by shearing faults/mega-fractures. Two inclined opposing systems of disturbances (type X) are distinguished, with angles of inclination of about 45°. Sporadically, there are individual subvertical breakaway faults. All disturbance systems are in good agreement with the zones of increased values of azimuthally anisotropic

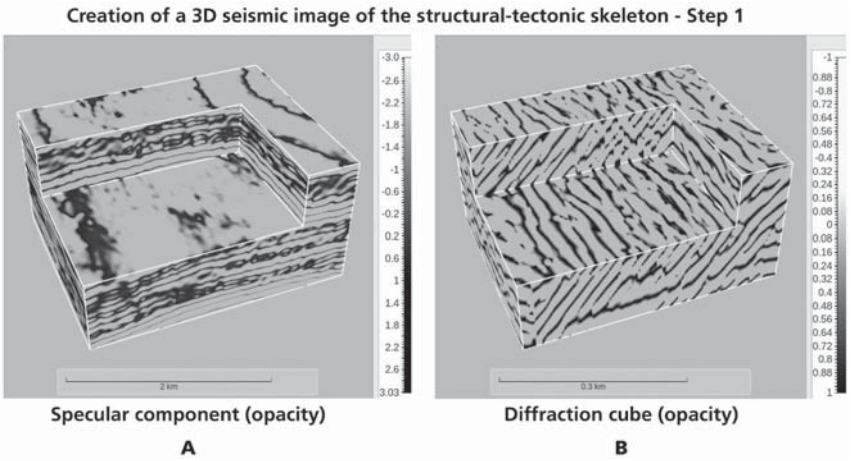

Figure 11 Creation of a 3D seismic image of the structural-tectonic skeleton (3D SI-STS). A: Specular image cube. B: Diffraction image cube. When rendering, image opacity is used.

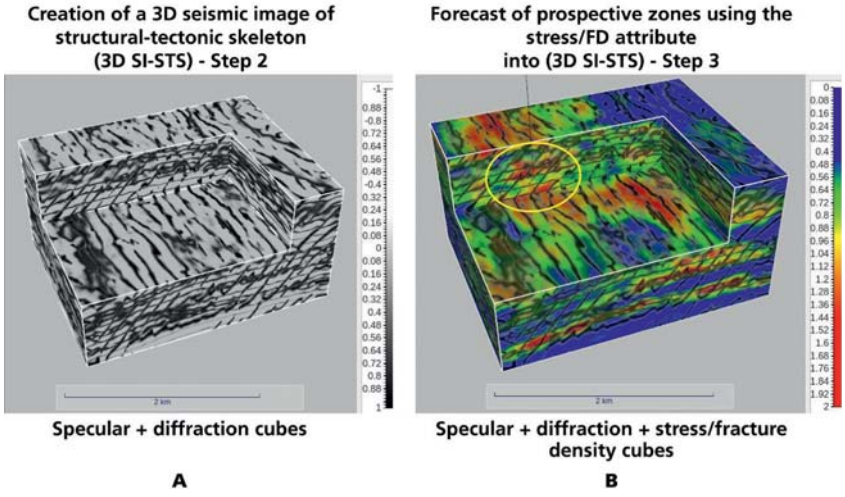

Figure 12 Creation of a 3D seismic image of a structural-tectonic skeleton (3D SI-STS). A: Combined cubes of specular and diffraction/corner wave components (SI-STS). B: Combined SI-STS cubes together with azimuthally anisotropic intensity.

intensity. In general, the overall picture of the disturbance systems identified using the new technology corresponds to the variant of the geomechanical model presented in the vertical section of Figure 8. In addition, two small circular objects are distinguished in the lower part of the Paleozoic basement (Devonian period), which may be either small atolls or karstic sinkholes.

Figure 14 shows the result of applying this technology to obtain an integrated cube from adjacent sections. We see that the selected inclined fault systems and seismic horizons almost

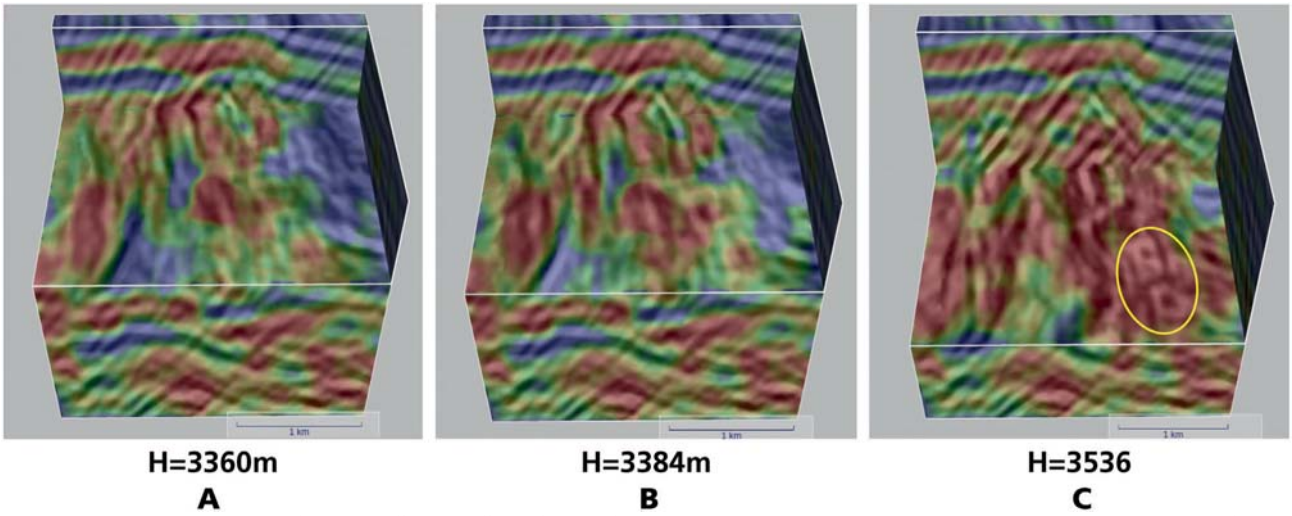

Figure 13 3D integrated interpretation: Specular + diffraction (diffractor filter workflow) + azimuthally anisotropic intensity cubes. A: Depth section in the upper part of the Paleozoic basement. B: Middle part of the Paleozoic basement. C: Lower part of the Paleozoic basement. The cube of the specular and diffraction components is obtained using the prestack technology of adaptive selection and removal of the specular energy.

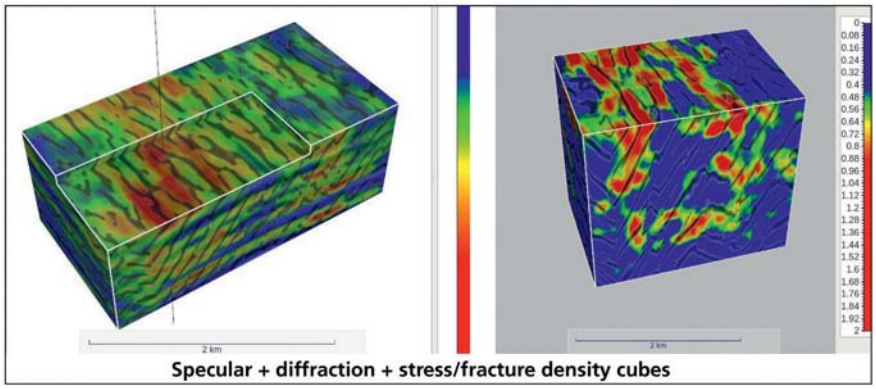

Figure 14 3D integrated interpretation.

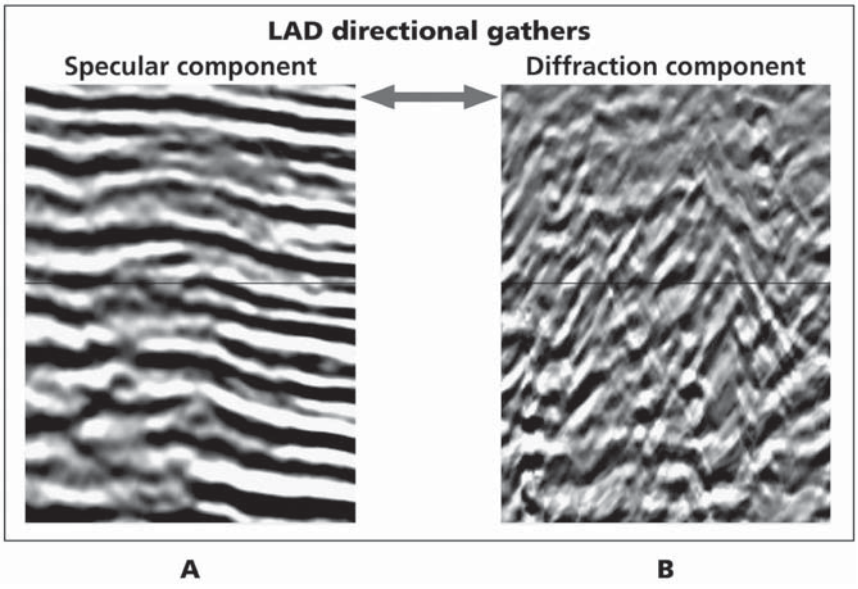

Figure 15 Example of separation of the wave field into directional gathers in a complex carbonate. A: Vertical section of the specular component cube. B: Diffraction/corner wave cube.

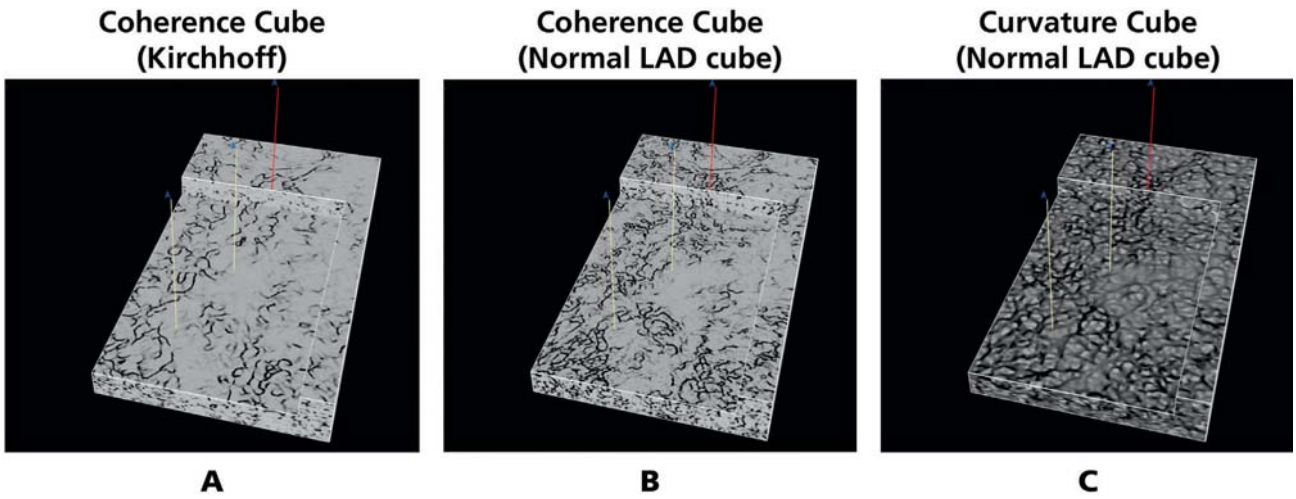

Figure 16 Details of heterogeneities in the barrier reef using different poststack methods for identifying heterogeneities. A: Coherence Cube — Kirchhoff migration. B: Coherence Cube — normal LAD cube. C: Curvature Cube — normal LAD cube. The red vertical line is a productive oil well. The yellow lines signify two unproductive wells.

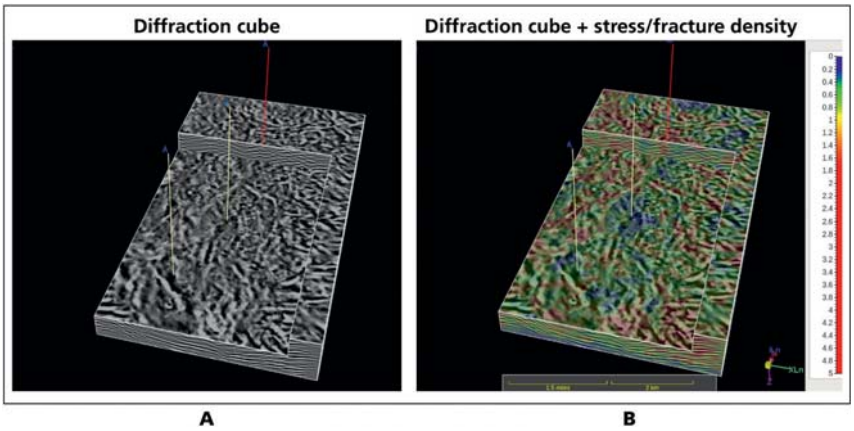

Figure 17 Details of heterogeneities within the barrier reef using different prestack methods for identifying heterogeneities. Diffractor (filter workflow) + anisotropy intensity. A: Combined cubes of specular and diffraction components (SI-STS). B: Combined SI-STS cubes and stress/fracture density.

completely control the distribution of blocks with anomalous intensities of the azimuthal anisotropy.

Middle Volga region

Oil-bearing reservoirs in the Middle Volga region also have hard-to-recover reserves (complex geological structure, small reservoir size with a complex distribution of fractured zones, low permeability of the cracked matrix, etc.). In this region, the search targets are oil-bearing carbonate reservoirs (reef structures) that are located in the carbonate strata at a depth of 3000-4000 m.

Figure 15 shows the result of a specular cube and diffraction/corner components obtained using the new prestack technology of adaptive selection and removal of the specular energy. It can be seen that the specular component (A) carries information only about continuous reflecting horizons, while the diffraction component (B) carries information about heterogeneities, mainly faults and mega-cracks. In the diffraction component section two opposite inclined systems of type X disturbances, which can control the shape and size of the oil and gas reservoirs, are distinguishable.

Figure 16 compares the results of the various technologies for identifying the main fault systems that control zonation of the barrier reef and potential oil-fractured reservoirs. The best result is in the Curvature Cube, calculated on the LAD normal cube (C). Here, the faults are more pronounced, resembling the shape of the cobble structure.

The most plausible result (Figure 17A) for identifying the main fault system is obtained using the new prestack extraction technology and adaptive removal of the specular energy described above. This is the only technology that provides an accurate and plausible image of the main fault system, in the form of linear orthogonal segments. It is along this system that the bound and unconnected segments of the barrier reef are located. In other words, the geometry of the major fault system completely controls the reef structure zoning. Finally, the integrated image of the structural-tectonic skeleton (SI-STS) and stress/fracture density cube provides complete clarity into the distribution of possible fractured zones in carbonate reservoirs (Figure 17B). These fractured zones are located along the main faults and geometrically repeat their outlines. A productive well (red) falls into the zone of anomalous values of the azimuthally anisotropic intensity (or stress/fracture density). Unproductive wells (yellow) fall into zones of low (or non-existent) azimuthally anisotropic intensity and are located at a considerable distance from the main faults, forming the geometry of the barrier reef.

Conclusion

In this article we have demonstrated an advanced processing, imaging and characterization system operating directly in the local angle domain (LAD) over two oil fields with different geo-

logical settings. Using directional image gathers, we were able to clearly decompose the full image data into specular energy, which enhances the structural continuity, as well as diffraction energy, for enhancing small and discontinuous subsurface objects, in particular fracture systems. This, in turn, provides geologists with a high-quality seismic image of the tectonic skeleton, which largely determines the shape and location of actual oil and gas reservoirs, particularly those with hard-to-recover reserves.

The specular weighted full-azimuth opening (reflection) angle gathers were optimally used for highly accurate, high-resolution VVAZ and AVAZ analysis, mainly to further characterize the azimuthally anisotropic effects associated with the target fracture systems.

This integrated analysis has proved to be a reliable basis for the final interpretation and construction of the geological model. It also fit well with the proposed geomechanical model, increasing understanding of the formation and structure of hydrocarbon reservoirs with hard-to-recover reserves. It should be noted that this technology is quick and easy to use. Integrated with stress/fracturing assessment information, the technology helps geoscientists to more reliably delineate oil and gas reservoirs.

Acknowledgement

The authors of the article are grateful to the management of HMNGGR and SINTEZ for the opportunity to evaluate new Paradigm technologies using their data.

References

Koren Z. and Rave I. [2011]. Full azimuth subsurface angle domain wavefield decomposition and imaging Part 1 and 2. *Geophysics*, **76** (part 1 and 2).

Kozlov, E.A., Koren, Z., Tverdohlebov, D.N. and Badeikin, A.N. [2009]. Corner reflectors – a new concept of imaging vertical boundaries. *71st EAGE Conference and Exhibition*, Extended Abstracts, Z039.

Khaidukov, V., Landa, E. and Moser, T.J. [2004]. Diffraction imaging by focusing-defocusing: An outlook on seismic superresolution. *Geophysics*, **69**, 1478-1490.

Benfield, N., Guise, A. and Chase, D. [2016]. Diffraction imaging – a tool to reduce exploration and development risk. *First Break*, **34**, 57-63.

Kowalski, H., Godlewski, P., Kobusinski, W., Makarewicz, J., Podolak, M., Nowicka, A. and Koren, Z. [2014]. Imaging and characterization of a shale reservoir onshore Poland, using full-azimuth seismic depth imaging. *First Break*, **32**, 101-109.

Inozemtsev, A., Koren, Z. and Galkin, A. [2015]. Noise suppression and multiple attenuation using full-azimuth angle domain imaging: case studies. *First Break*, **33**, 81-86.

de Ribet, B., Yelin, G., Serfaty, Y., Chase, D., Kelvin, R. and Koren, Z. [2017]. High resolution diffraction imaging for reliable interpretation of fracture systems. *First Break*, **35**, 43-37.

Inozemtsev, A., Stepanov, I., Galkin, A. and Koren, Z. [2013]. Applying full–azimuth angle domain pre-stack migration and AVAZ inversion to study fractures in carbonate reservoirs in the Russian Middle Volga region. *First Break*, **31**, 79-84.

Moser, T.J. and Howard, C.B. [2008]. Diffraction imaging in depth. *Geophysical Prospecting*, **56**, 627-641

Ivanov, K.S., Yu, V., Erokhin, V.B., Pisetsky, V.S. Ponomareov, and O.E. Pogromskaya. [2012]. New data on the structure of the West-Siberian Platform basement. *Journal of Lithosphere*, 4.

Kontorovich, V.A. [1999]. History of tectonic evolution of southeastern West Siberia in Jurassic period. *Journal Geology of Oil and Gas.*

Yaschenko, I., Polishchuk, Y. and Kozin, E. [2015]. Difficult oil: Classification and analysis of qualitative features. *Oil & Gas Journal Russia.*

Chernyshev, S.N. [2003]. *Fractures of rocks*. Science, Nedra, Moscow.